TU Delft

Delft University of Technology

Adaptive compensation of measurement delays in multi-sensor fusion for inertial motion tracking using moving horizon estimation

Girrbach, Fabian; Kok, Manon; Zandbergen, Raymond; Hageman, Tijmen; Diehl, Moritz

DOI
10.23919/FUSION45008.2020.9190632

Publication date
2020

Document Version
Final published version

Published in
Proceedings of 2020 23rd International Conference on Information Fusion, FUSION 2020

Citation (APA)
Girrbach, F., Kok, M., Zandbergen, R., Hageman, T., & Diehl, M. (2020). Adaptive compensation of measurement delays in multi-sensor fusion for inertial motion tracking using moving horizon estimation. In *Proceedings of 2020 23rd International Conference on Information Fusion, FUSION 2020* Article 9190632 IEEE. https://doi.org/10.23919/FUSION45008.2020.9190632

Important note
To cite this publication, please use the final published version (if applicable).
Please check the document version above.

Copyright
Other than for strictly personal use, it is not permitted to download, forward or distribute the text or part of it, without the consent of the author(s) and/or copyright holder(s), unless the work is under an open content license such as Creative Commons.

Takedown policy
Please contact us and provide details if you believe this document breaches copyrights.
We will remove access to the work immediately and investigate your claim.

This work is downloaded from Delft University of Technology.
For technical reasons the number of authors shown on this cover page is limited to a maximum of 10.

Green Open Access added to TU Delft Institutional Repository

'You share, we take care!' - Taverne project

https://www.openaccess.nl/en/you-share-we-take-care

Otherwise as indicated in the copyright section: the publisher is the copyright holder of this work and the author uses the Dutch legislation to make this work public.

Adaptive compensation of measurement delays in multi-sensor fusion for inertial motion tracking using moving horizon estimation

Fabian Girrbach*, Manon Kok‡, Raymond Zandbergen*, Tijmen Hageman* and Moritz Diehl†
*Xsens Technologies B.V., 7521 PR Enschede, the Netherlands
Email: firstname.lastname@xsens.com
†Department of Microsystems Engineering (IMTEK), University of Freiburg, 79110 Freiburg, Germany,
Email: firstname.lastname@imtek.uni-freiburg.de
‡Department of Mechanical, Maritime and Materials Engineering, Technical University Delft, 2628 CD Delft, the Netherlands
Email: m.kok-1@tudelft.nl

***Abstract*—Robust and accurate pose estimation of moving systems is a challenging task that is often tackled by combining information from different sensor subsystems in a multi-sensor fusion setup. To obtain robust and accurate estimates, it is crucial to respect the exact time of each measurement. Data fusion is additionally challenged when the sensors are running at different rates and the information is subject to processing- and transmission delays. In this paper, we present an optimization-based moving horizon estimator which allows to estimate and compensate for time-varying measurement delays without the need for any synchronization signals between the sensors. By adopting a direct collocation approach, we find a continuous-time solution for the navigation states which allows us to incorporate the discrete-time sensor measurements in an optimal way despite the presence of unknown time delays. The presented sensor fusion algorithm is applied to the problem of pose estimation by fusing data of a high-rate inertial measurement unit and a low-rate centimeter-accurate global navigation satellite system receiver using simulated and real-data experiments.**

***Index Terms*—State estimation, sensor fusion, multi-sensor, direct collocation, MHE, IMU, RTK, GNSS.**

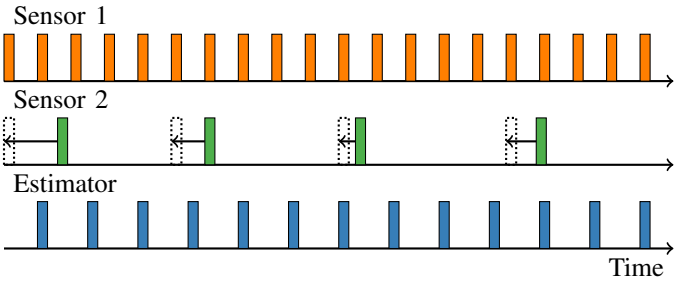

Fig. 1. Schematic drawing showing the arrival of data in a multi-rate sensor fusion setup. The first axis represents a high-rate sensor with very deterministic measurement behavior, which is typical for a low-level sensor e.g. an IMU or an encoder. The second axis represents a low-rate sensor of which measurements take longer to process and therefore suffer from an unknown and varying delay. Such behavior could be expected from a visual odometry sensor or other positioning sensors. The last axis shows the output of the state estimator where its rate is often desired to coincide with the rate of the control system.

I. Introduction

In recent years, several key technologies in the field of pose estimation and localization have matured and are now available as independent subsystems [1]. Such systems are for instance based on *global navigation satellite system* (GNSS) receivers, cameras or range sensors to determine the pose of the moving system. To achieve a high robustness or simply to increase accuracy, these sensor technologies are often combined with each other or with additional sensors, e.g. *inertial measurement unit*s (IMUs) or internal encoders in a multi-sensor fusion setup. The combination of several sensors raises typically three issues which are also visualized in Fig. 1. Firstly, the independent subsystems do not share a common clock and a synchronization using trigger signals is likely to result in a cumbersome electronic design and is sometimes simply not possible. Secondly, the integrated data processing and transmission of the data itself causes additional time delays until the required information arrives at a central node on which all the measurements are fused in a sensor fusion algorithm. Thirdly, different sensors typically sample at different rates, resulting in a multi-rate sensor fusion problem. The result is a very complex sensory- and perception system of which its estimation performance is prone to degradation if the mentioned issues are not properly handled.

A practical solution to cope with unknown time delays can be noise boosting, which can reduce the unwanted impact of the delay on the estimation results by sacrificing the overall estimation accuracy. Several approaches have been published which aim to improve the estimation performance by considering presence of time delays in their estimation algorithm. Uncertain measurement delays with low variance can be incorporated into the well known *extended Kalman filter* (EKF) framework [2] by adding a buffer to the recursive

This work was started during the project AWESCO (H2020-ITN-642682) funded by the European Union's Horizon 2020 research and innovation program under the Marie Skłodowska-Curie grant agreement No. 642682.

Authorized licensed use limited to: TU Delft Library. Downloaded on March 16,2022 at 12:47:23 UTC from IEEE Xplore. Restrictions apply.

filter containing a history of states and measurements. The buffered information is used to compute partial updates of the state until the point that all information is available. To ensure optimality the authors use an iterative strategy commonly referred to as *iterated* EKF (IEKF). Unknown measurement delays are compensated in [3] up to a delay of the fastest sampled sensor in a linear filter, designed to estimate position and velocity of an aerial vehicle. In [4] the discrete *Kalman filter* (KF) compensates known time delays by extrapolating the measurement information to the required time. Two main different algorithmic approaches are identified in [5], where the authors group EKF-based approaches based on the usage of state augmentation or modified update equations which process the delayed information as soon it becomes available. Recently, a *moving horizon estimation* (MHE)-based estimator was proposed in [6] which is limited to linear systems and therefore not applicable to many problems in navigation and robotics. A possible extension of this idea to nonlinear systems by will degrade the estimation performance in the presence of linearization errors.

In this paper, we present a multi-sensor fusion approach which is able to compensate for measurement delays and relax the requirement of a precise synchronization between subsystems as illustrated in Fig. 1. This work is specifically suited for loosely-coupled sensor fusion setups where the onboard data processing on each subsystem significantly increases the delay. The presented algorithm is based on finding an approximate continuous-time solution to the naturally discrete-time estimation problem by applying the concept of direct collocation to the MHE framework. This allows us to identify the actual time of the measurement and hence achieve accurate estimation results, regardless of time delays or unknown timestamps by minimizing over the continuous control and state space. In Section II, we describe the estimation framework allowing for adaptive delay compensation in a general way. The framework is then used in Section III for the compensation of measurement delays of a centimeter-accurate GNSS receiver using the *real time kinematics* (RTK) technology and an IMU. Finally, we evaluate the designed estimator in Sections IV and V using simulated and real measurement data, respectively.

II. Adaptive delay compensation using MHE

In order to introduce our approach for adaptive delay compensation using MHE, we first review the standard discrete-time formulation of MHE and introduce the concept of direct collocation before defining our novel MHE approach.

A. Discrete-time MHE

MHE is an approach for online nonlinear state estimation which aims to yield accurate estimation solutions by formulating a possibly constrained nonlinear optimization problem using measurement data from the recent past [7]. The measurements capture information at discrete times t_k, which makes the discretization of state and control spaces a natural choice. The estimation horizon length $N \in \mathbb{N}$ is defined by the number of discretized states which are considered in the estimation window and is often directly related to the number of measurements. We use the index K to indicate the start of the estimation window at time $t_K = t_{k-N}$ which is shifted over time keeping the horizon length constant. For a simple MHE estimator such an optimization problem can be defined as:

$$\min_{\substack{\boldsymbol{x}_{K:K+N} \\ \boldsymbol{u}_{K:K+N-1}}} \quad \|\boldsymbol{x}_K - \bar{\boldsymbol{x}}_K\|^2_{\mathcal{A}_K} + \sum_{k=K+1}^{K+N} \|h(\boldsymbol{x}_k, \boldsymbol{u}_{k-1}) - \boldsymbol{z}_k\|^2_{\mathcal{R}_k} + \\ + \sum_{k=K}^{K+N-1} \|g(\boldsymbol{u}_k, \boldsymbol{x}_k) - \bar{\boldsymbol{u}}_k\|^2_{\mathcal{Q}_k} \tag{1a}$$

$$\text{s.t.} \quad \boldsymbol{x}_{k+1} = F(\boldsymbol{x}_k, \boldsymbol{u}_k),\ k = K, \dots, K+N-1, \tag{1b}$$

where the objective function (1a) is defined by the weighted quadratic residual between measurements $\boldsymbol{z} \in \mathbb{R}^{N_{\boldsymbol{z}}}$ of dimension $N_{\boldsymbol{z}} \in \mathbb{N}$ and the possibly nonlinear measurement model $h(\boldsymbol{x}, \boldsymbol{u})$. A further possibly nonlinear function $g(\boldsymbol{u}, \boldsymbol{x})$ is used to model the relation between the controls $\boldsymbol{u} \in \mathbb{R}^N_{\boldsymbol{u}}$ and the measured controls $\bar{\boldsymbol{u}} \in \mathbb{R}^N_{\boldsymbol{u}}$. The described cost term models the uncertainty of the control inputs which can be considered alternatively using additional process noise variables [8]. The residuals are weighted according to the inverse of the measurement and control noise matrices $\mathcal{R} \in \mathbb{R}^{N_{\boldsymbol{z}} \times N_{\boldsymbol{z}}}$ and $\mathcal{Q} \in \mathbb{R}^{N_{\boldsymbol{u}} \times N_{\boldsymbol{u}}}$. Knowledge about the past enters the problem by using a quadratic arrival cost term on $\boldsymbol{x}_K$ and $\bar{\boldsymbol{x}}_K$ which is weighted by the matrix $\mathcal{A}_K \in \mathbb{R}^{N_{\boldsymbol{x}} \times N_{\boldsymbol{x}}}$. Note that $\bar{\boldsymbol{x}}_K$ is a constant and not an optimization variable. The dynamic system model enters in this formulation by imposing multiple shooting constraints (1b), where $F(\boldsymbol{x}, \boldsymbol{u})$ defines an integrator function which depends on the state value $\boldsymbol{x}$ and control input $\boldsymbol{u}$ and the *ordinary differential equation* (ODE) of the system.

B. Direct collocation

In order to account for delayed measurement information, a discrete-time formulation of the estimation problem is not suitable. We need a continuous-time representation of the state $\boldsymbol{x}(t)$ allowing us to evaluate the measurement models at every point in time t. In this work, we use a direct collocation approach using Lagrange polynomials which encode the state trajectory between t_k and t_{k+1}. By embedding a polynomial interpolation method of the state trajectory inside the optimization problem, we can propagate the state according to the dynamics of the system and at the same time get a continuous representation of the state. We use $D \in \mathbb{N}$ orthogonal polynomials at Radau (aka Gauss-Radau or Legendre-Gauss-Radau) collocation points $c_{1:D} \in [0, 1]$ [9]. Each polynomial of degree $D \in \mathbb{N}$ is therefore defined by

$$P_{k,d}(\tau; c_{1:D}) = \prod_{i=1, j \neq i}^{D} \frac{\tau - c_i}{c_j - c_i}, \qquad 0 \leq \tau \leq 1, \tag{2}$$

where the subindex i, j refers to the respective collocation point and τ is the evaluation point. Note that we use a ; to separate the variable function arguments from constant parameters. The continuous-time representation of controls

Authorized licensed use limited to: TU Delft Library. Downloaded on March 16,2022 at 12:47:23 UTC from IEEE Xplore. Restrictions apply.

and states is defined by the sum of the individual polynomials yielding the following functions for the evaluation of both trajectories. The control function

$$\Phi(\tau, \boldsymbol{u}_{k,1:D}; c_{1:D}) = \sum_{i=1}^{D} \boldsymbol{u}_{k,i} P_{k,i}(\tau; c_{1:D}), \quad 0 \leq \tau \leq 1, \quad (3)$$

uses D collocation variables denoted by $\boldsymbol{u}_{k,1:D}$ to evaluate the value of the controls at the normalized time τ which is valid for the interval $[t_k, t_{k+1}]$. To integrate the ODE of the system a further collocation point is added at the beginning of the interval yielding $\boldsymbol{x}_{k,0:D}$ collocation variables and a higher polynomial degree $D+1$. We define the state function and its first derivative w.r.t time as

$$\Psi(\tau, \boldsymbol{x}_{k,0:D}; c_{0:D}) = \sum_{i=0}^{D} \boldsymbol{x}_{k,i} P_i(\tau; c_{0:D}), \ 0 \leq \tau \leq 1, \quad (4a)$$

$$\dot{\Psi}(\tau, \boldsymbol{x}_{k,0:D}; c_{0:D}) = \sum_{i=0}^{D} \boldsymbol{x}_{k,i} \dot{P}_i(\tau; c_{0:D}), \ 0 \leq \tau \leq 1, \quad (4b)$$

respectively. Since it might not be required to get continuous trajectories for all the states contained in the vector $\boldsymbol{x}$, we redefine $\boldsymbol{x} \in \mathbb{R}^{N_{\boldsymbol{x}_c}}$ to only contain the collocation and therefore continuous states. The discrete states are contained in $\boldsymbol{s} \in \mathbb{R}^{N_{\boldsymbol{x}_s}}$ leading to $N_{\boldsymbol{x}} = N_{\boldsymbol{x}_c} + N_{\boldsymbol{x}_s}$.

C. Delay estimation & compensation using MHE

Despite (1) being a simple MHE problem, the standard discrete-time definition of MHE bases on the assumption that all measurements entering the computation of the residuals are sharing common sampling times t_k. In a loosely-coupled multi-sensor fusion setup such an assumption is very likely to be violated due to unknown processing and communication delays.

Adopting the presented collocation strategy to MHE, it is possible to estimate the continuous time delay resulting in the optimization problem (6), where we adapted the optimization variables in comparison to (1) to include the collocation variables for the continuous states $\boldsymbol{x}$ and controls $\boldsymbol{u}$. Furthermore, we introduce the discrete states $\boldsymbol{s}$ and the variables for the time of measurement τ_k as optimization variables. The role of the arrival cost is unchanged besides splitting the state vector into continuous and discrete states. The measurement residual term makes use of the state and control functions, (4a) and (3), respectively, for which we estimate the time of measurement τ_k by minimizing the residual along the state and control trajectories. The control residual term makes use of the same functions but we added an additional sum to incorporate $M \in \mathbb{N}$ high rate control inputs at known normalized sampling times $t_{0:M} \in [0, 1]$. Note that this term by itself represents an independent *weighted least squares* (WLS) fit, if and only if $g(\cdot)$ is independent of $\boldsymbol{x}$ and can be solved in such case beforehand. The last term in the objective function models the evolution over time of the discrete states $\boldsymbol{s}$ as e.g. a random walk process. Radau points share the property of having a node at the end of the interval which simplifies the shooting constraints in (6b). The system dynamics enter the problem over the collocation constraints (6c), where the derivative of the state trajectory (4a) is set equal to the ODE of the system $f(\cdot)$ at the collocation nodes. Finally, the inequality constraint (6d) ensures that τ_k stays in a valid range.

III. Inertial motion tracking with delayed position updates

We want to motivate the benefit of the presented approach with a practical example from GNSS-aided inertial motion tracking, where the low-rate position measurements of a GNSS receiver are used to compensate the drift of the IMU, which is caused by measurement noise and biases. The fusion of IMU and GNSS is a well studied topic [10], but technological advances which lead to more accurate measurement information impose also new challenges. The typical measurement accuracy of a single GNSS receiver is around 2 m which masks the effects of modeling errors such as time delays. Time delays contribute generally to a position error scaling linearly with the velocity of the system. The increasing demand for centimeter accurate positioning is addressed with the RTK-GNSS technology which uses correction information from local base stations to correct in real-time for atmospheric errors in the GNSS signals. The additional correction messages increase the computational burden for the GNSS receiver causing larger processing delays, while the improved positioning accuracy is more severely affected by modeling errors.

$$\underset{\substack{\boldsymbol{x}_{K:K+N,0:D} \\ \boldsymbol{u}_{K:K+N-1,1:D} \\ \boldsymbol{s}_{K:K+N} \\ \tau_{K:K+N-1}}}{\text{minimize}} \quad \left\| \begin{bmatrix} \boldsymbol{x}_{K,D} \\ \boldsymbol{s}_K \end{bmatrix} - \begin{bmatrix} \bar{\boldsymbol{x}}_K \\ \bar{\boldsymbol{s}}_K \end{bmatrix} \right\|^2_{\mathcal{A}_K} + \sum_{k=K+1}^{K+N} \| h(\Psi(\tau_k, \boldsymbol{x}_{k,0:D}), \Phi(\tau_k, \boldsymbol{u}_{k-1,1:D})) - \boldsymbol{z}_k \|^2_{\mathcal{R}_k} +$$

$$+ \sum_{k=K}^{K+N-1} \sum_{m=0}^{M} \| g(\Psi(t_m, \boldsymbol{x}_{k,0:D}), \Phi(t_m, \boldsymbol{u}_{k,1:D})) - \bar{\boldsymbol{u}}_k \|^2_{\mathcal{Q}_m} + \| \lambda(\boldsymbol{s}_k) - \boldsymbol{s}_{k+1} \|^2_{\mathcal{S}_k} \quad (6a)$$

$$\text{subject to} \quad \boldsymbol{x}_{k+1,0} = \boldsymbol{x}_{k,D}, \qquad k = K, \ldots, K+N-1, \quad (6b)$$

$$\dot{\Psi}(c_d, \boldsymbol{x}_{k,0:D}) = f(\boldsymbol{x}_{k,d}, \boldsymbol{u}_{k,d}), \qquad d = 1, \ldots, D, \ k = K, \ldots, K+N-1, \quad (6c)$$

$$0 \leq \tau_k \leq 1, \qquad k = K, \ldots, K+N-1. \quad (6d)$$

Authorized licensed use limited to: TU Delft Library. Downloaded on March 16,2022 at 12:47:23 UTC from IEEE Xplore. Restrictions apply.

In the following, we will define the models according to the definitions in Section II.

A. Models

To allow the estimation of position, velocity, and orientation using position and inertial, i.e., angular rate and specific force, measurements, we start by the definition of the controls, continuous, and discrete states, $\boldsymbol{u}$, $\boldsymbol{x}$, and $\boldsymbol{s}$, respectively

$$\boldsymbol{x} = \left[{}^{\mathrm{L}}p^{\mathrm{T}}, {}^{\mathrm{L}}v^{\mathrm{T}}, {}^{\mathrm{LS}}q^{\mathrm{T}} \right]^{\mathrm{T}}, \tag{5a}$$

$$\boldsymbol{s} = \left[{}^{\mathrm{S}}_{\mathrm{a}}\delta^{\mathrm{T}}, {}^{\mathrm{S}}_{\mathrm{g}}\delta^{\mathrm{T}} \right]^{\mathrm{T}}, \tag{5b}$$

$$\boldsymbol{u} = \left[{}^{\mathrm{S}}f^{\mathrm{T}}, {}^{\mathrm{S}}_{\mathrm{LS}}\omega^{\mathrm{T}} \right]^{\mathrm{T}}, \tag{5c}$$

where the position ${}^{\mathrm{L}}p \in \mathbb{R}^3$ and velocity ${}^{\mathrm{L}}v \in \mathbb{R}^3$ of the system are expressed with respect to the local and non-moving frame L. The orientation between the fixed L and moving sensor frame S is described by the unit quaternion ${}^{\mathrm{LS}}q \in \{\mathbb{R}^4 \mid \left\| {}^{\mathrm{LS}}q \right\|^2 = 1\}$ [11]. We further estimate as discrete states the biases of the IMU sensors which are defined by ${}^{\mathrm{S}}_{\mathrm{a}}\delta \in \mathbb{R}^3$ for accelerometer and ${}^{\mathrm{S}}_{\mathrm{g}}\delta \in \mathbb{R}^3$ for gyroscope triads. The ODE of the state is driven by the control vector $\boldsymbol{u}$ containing the angular velocity ${}^{\mathrm{S}}_{\mathrm{LS}}\omega \in \mathbb{R}^3$ between the S-and L-frame and the free acceleration ${}^{\mathrm{S}}f \in \mathbb{R}^3$, both observed in the S-frame leading to

$$f(\boldsymbol{x}, \boldsymbol{u}) \coloneqq \frac{d}{dt}\boldsymbol{x} = \frac{d}{dt}\begin{bmatrix} {}^{\mathrm{L}}p \\ {}^{\mathrm{L}}v \\ \log {}^{\mathrm{LS}}q \end{bmatrix} = \begin{bmatrix} {}^{\mathrm{L}}v \\ R_{{}^{\mathrm{LS}}q}\, {}^{\mathrm{S}}f \\ {}^{\mathrm{S}}_{\mathrm{LS}}\omega \end{bmatrix} \tag{7}$$

where the free acceleration ${}^{\mathrm{S}}f$ is rotated to the L-frame using the rotation matrix $R_{{}^{\mathrm{LS}}q} \in \mathbb{R}^{3\times3}$ to express the time derivative of ${}^{\mathrm{L}}v$. Notice the use of the logarithmic map to express the time derivative of the orientation state ${}^{\mathrm{LS}}q$ [12]. The biases ${}^{\mathrm{S}}_{\mathrm{a}}\delta$, ${}^{\mathrm{S}}_{\mathrm{g}}\delta$ are modeled as random walk processes and therefore (6a) simplifies to $\lambda(\boldsymbol{s}_k) = \boldsymbol{s}_k$. The resulting residual is weighted by $\mathcal{S} = \operatorname{diag}\left[\nu_{\mathrm{acc}}^{\mathrm{T}}, \nu_{\mathrm{gyr}}^{\mathrm{T}}\right]^{-2} \in \mathbb{R}^{6\times6}$ containing the corresponding random walk variances for accelerometer and gyroscope. We define the measurement models $h(\cdot)$ to predict measurements using the polynomial evaluation functions for state (4a) and controls (3) to compute the arguments of

$$h(\boldsymbol{x}_k, \boldsymbol{u}_k) = h({}^{\mathrm{L}}p, {}^{\mathrm{LS}}q; {}^{\mathrm{S}}\iota) = {}^{\mathrm{L}}p + R_{{}^{\mathrm{LS}}q}\, {}^{\mathrm{S}}\iota. \tag{8}$$

The model accounts for the lever arm ${}^{\mathrm{S}}\iota \in \mathbb{R}^3$ of the GNSS antenna respective the IMU sensor. Notice, that ${}^{\mathrm{S}}\iota$ is defined in the S-frame and therefore rotated to the L-frame using $R_{{}^{\mathrm{LS}}q}$. The measurement residual in (6) is weighted according to the standard deviation of the GNSS receiver $\mathcal{R} = \operatorname{diag}\left[\sigma_{\mathrm{gnss}}\right]^{-2} \in \mathbb{R}^{3\times3}$.

The control input model $g(\cdot)$ defines the relation between IMU measurements and control signals $\boldsymbol{u}$.

$$g(\boldsymbol{x}, \boldsymbol{u}) = g({}^{\mathrm{S}}f, {}^{\mathrm{S}}_{\mathrm{LS}}\omega, {}^{\mathrm{S}}_{\mathrm{a}}\delta, {}^{\mathrm{S}}_{\mathrm{g}}\delta) = \begin{bmatrix} {}^{\mathrm{S}}f + R_{{}^{\mathrm{SL}}q}\, {}^{\mathrm{L}}g + {}^{\mathrm{S}}_{\mathrm{a}}\delta \\ {}^{\mathrm{S}}_{\mathrm{LS}}\omega + {}^{\mathrm{S}}_{\mathrm{g}}\delta \end{bmatrix}, \tag{9}$$

where we rotate the local gravity ${}^{\mathrm{L}}g \in \mathbb{R}^3$ to the S-frame and add the free acceleration signal ${}^{\mathrm{S}}f$. The residual in (6) is weighted according to the standard deviation calculated from the noise density for accelerometer and gyroscope $\mathcal{Q} = \operatorname{diag}\left[\sigma_{\mathrm{acc}}^{\mathrm{T}}, \sigma_{\mathrm{gyr}}^{\mathrm{T}}\right]^{-2} \in \mathbb{R}^{6\times6}$.

B. Implementation

In the described application, we estimate the orientation of the sensor w.r.t to a fixed frame L. To represent the 3 degrees of freedom of the orientation, we use unit quaternions ${}^{\mathrm{LS}}q$ which represent an over-parameterization to avoid singularities. For valid orientation estimates it is crucial to optimize on a valid orientation manifold of unit quaternions. In this work, we follow the approach described in [12], by making extensive use of the logarithmic and exponential map. While the sensor and control models, (8) and (9) respectively, use the value of the quaternion ${}^{\mathrm{LS}}q$, the shooting constraints (6b) and the optimizer use the logarithmic map.

The approach is implemented in the Python computing language and uses algorithmic differentiation to calculate residuals and derivatives of cost functions and constraints. This information is fed to the open-source interior point solver IPOPT [13] using the Gauss-Newton approximation to ensure a positive-definite Hessian [14].

IV. Simulation Results

We randomly generate datasets containing ground-truth and sensor data using the simulation approach described in [15]. The simulation framework uses random waypoints in orientation and position together with interpolation techniques to generate smooth motion trajectories reflecting realistic system dynamics. The original approach was extended to allow the insertion of artificial time delays of the sensor measurements. Table I summarizes the simulation parameters and sensor parameters such as sampling rates $\mathcal{F}$, noise densities η, biases δ, and the lever arm ${}^{\mathrm{S}}\iota$ of the GNSS antenna. Values which are sampled from distributions are denoted by $\mathcal{N}$ and $\mathcal{U}$, for normal and uniform distributions, respectively. The delay of the GNSS measurements is uniformly sampled over the interval $[0, 0.25]$ s and considered constant. The selected noise parameters of the IMU are typical for a low-grade consumer device which can be found in smartphones or other consumer electronics.

The 20 simulated datasets, each containing 30 s of sensor data, are used to evaluate the performance of the described approach. The estimator output rate $\mathcal{F}_{\mathrm{est}}$ is set to 4 Hz for this evaluation which is equal to the rate of the GNSS sensor. Therefore, the time of the GNSS measurement always lies inside the time interval which is represented by one collocation interval. If the estimator rate is desired to be higher, we propose to check for active inequality constraints of τ (6d) after convergence and shift the measurement to the previous collocation interval if the length of horizon allows this operation.

The estimator is initialized by setting the estimates of the IMU biases, the initial velocity, and the heading or yaw angle to 0. Pitch and roll angles are initialized using the first accelerometer measurement [16]. Under the assumption that

Authorized licensed use limited to: TU Delft Library. Downloaded on March 16,2022 at 12:47:23 UTC from IEEE Xplore. Restrictions apply.

TABLE I
SIMULATION PARAMETERS IN TERMS OF VALUE OR SAMPLING DISTRIBUTION.

	Parameter	Value	Unit
Waypoints	${}^{\mathrm{L}}p$	$\mathcal{N}(0, [5, 5, 1]^{\mathrm{T}})$	m
	${}^{\mathrm{LS}}q$	$\mathcal{N}(0, [10, 10, 80]^{\mathrm{T}})$	deg
Accelerometer	$\mathcal{F}_{\mathrm{acc}}$	400	Hz
	η_{acc}	180	$\mu\mathrm{g}\sqrt{\mathrm{Hz}}^{-1}$
	${}^{\mathrm{S}}_{\mathrm{a}}\delta$	$\mathcal{N}(0, 0.125)$	$\mathrm{m\,s}^{-2}$
Gyroscope	$\mathcal{F}_{\mathrm{gyr}}$	400	Hz
	η_{gyr}	0.007	$\mathrm{deg\,s}^{-1}\sqrt{\mathrm{Hz}}^{-1}$
	${}^{\mathrm{S}}_{\mathrm{g}}\delta$	$\mathcal{N}(0, 0.15)$	$\mathrm{deg\,s}^{-1}$
GNSS	$\mathcal{F}_{\mathrm{gnss}}$	4	Hz
	σ_{gnss}	$\mathcal{N}(0, [2, 2, 4]^{\mathrm{T}})$	cm
	${}^{\mathrm{S}}\iota$	$\mathcal{N}(0, [1.5, 1.5, 1]^{\mathrm{T}})$	m
	τ_{gnss}	$\mathcal{U}([0, 25])$	s

TABLE II
STANDARD DEVIATIONS FOR THE INITIALIZATION OF THE ESTIMATOR.

State	σ_0	Unit
${}^{\mathrm{LS}}q_{0,0}$	$[10, 10, 50]$	deg
${}^{\mathrm{L}}p_{0,0}$	$[1, 1, 1]$	m
${}^{\mathrm{L}}v_{0,0}$	$[0.1, 0.1, 0.1]$	$\mathrm{m\ s}^{-1}$
${}^{\mathrm{S}}_{\mathrm{a}}\delta_{0,0}$	$[0.15, 0.15, 0.15]$	$\mathrm{m\ s}^{-2}$
${}^{\mathrm{S}}_{\mathrm{g}}\delta_{0,0}$	$[0.15, 0.15, 0.15]$	$\mathrm{deg\ s}^{-1}$

the device is static at startup, the measured gravity vector allows for a reasonable initialization of pitch and roll angles. The initial state values are used to construct a prior using the corresponding standard deviations which are summarized in Table II.

Fig. 2 shows the *root mean square error* (RMSE) between the estimated position and the simulated ground truth trajectory. We evaluate each dataset for different horizons $N = \{1, 2, 3, 4, 5, 10\}$ yielding a maximum measurement history of 2.5 s for the MHE estimator. Additionally, we run each experiment with the delay compensation active and disabled, which means for the latter that we use the time when the GNSS data arrived and is therefore available in the data stream. By observing the results without delay compensation in Fig. 2, we notice how crucial it is to take the time delay into account. The simulated delays cause position errors in range of 20 cm despite using GNSS position measurements with an accuracy in the order of centimeters. By increasing the horizon N, the position errors slightly decrease but are still higher than expected from the simulated measurement accuracy. We observe that z-position errors are lower for all evaluated horizons. This behavior is explained by the simulated excitation which is responsible for moving the system mainly in the xy-plane (see Table I).

When enabling the delay compensation, the RMSE decreases

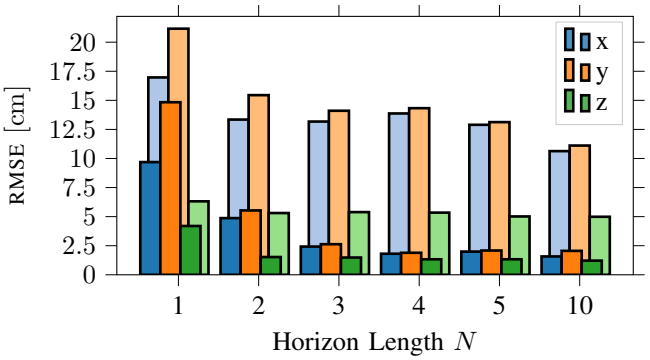

Fig. 2. RMSE of position estimates for simulated datasets for different horizon lengths with (*solid-colored*) and without (*light-colored*) the delay estimation enabled.

significantly for all evaluated horizons. Furthermore, we observe that the position errors decrease with an increasing estimation horizon yielding an accuracy of about 2 cm for all axes with a horizon of $N \geq 3$. Such an accuracy is desired when fusing position measurements of a similar accuracy.

By fusing position measurements with inertial measurements, the orientation can be observed. The RMSE of the orientation error estimates are visualized in Fig. 3 using Euler angles. In general, we observe that pitch and roll angles can be estimated with a higher accuracy than the yaw angle. This behavior is explained by measuring the gravity vector with the accelerometer which allows to observe the roll and pitch angle [16]. We can confirm this behavior by yielding errors below 1.25 deg for all horizons with and without delay estimation enabled. Regardless of this, we can show with Fig. 3, that enabling the delay estimation reduces the RMSE to up to 0.2 deg. Even more improvement, we see for the yaw angle which is not observable from the IMU data itself. By fusing the accurate position measurements at the correct instance in time, we can decrease the RMSE by one order of magnitude from around 10 deg to 1 deg. Notice that we are not gaining estimation performance if the delay estimation is disabled.

The detailed ground truth information allows us in Fig. 3 to evaluate the quality of the delay estimation itself for the simulated motion trajectories. The presented approach is capable to compensate varying measurement delays, yet in many practical applications the delay is observed to be nearly constant. Following this argumentation, we evaluate the estimator using a constant delay for each motion trajectory. The value of the measurement delay for each trial is uniformly sampled from the interval given in Table I. The resulting mean value of the simulated measurement delay over all datasets is visualized in Fig. 4 using a line plot. The RMSE of the estimated time delay is below σ_{sim} for all horizons and decreasing continuously for larger horizons. The RMSE converges to a value of 5 ms for a horizon $N \geq 5$. Furthermore, we notice the converging standard deviations of the estimation error for increasing horizons. Despite the higher accuracy of

Authorized licensed use limited to: TU Delft Library. Downloaded on March 16,2022 at 12:47:23 UTC from IEEE Xplore. Restrictions apply.

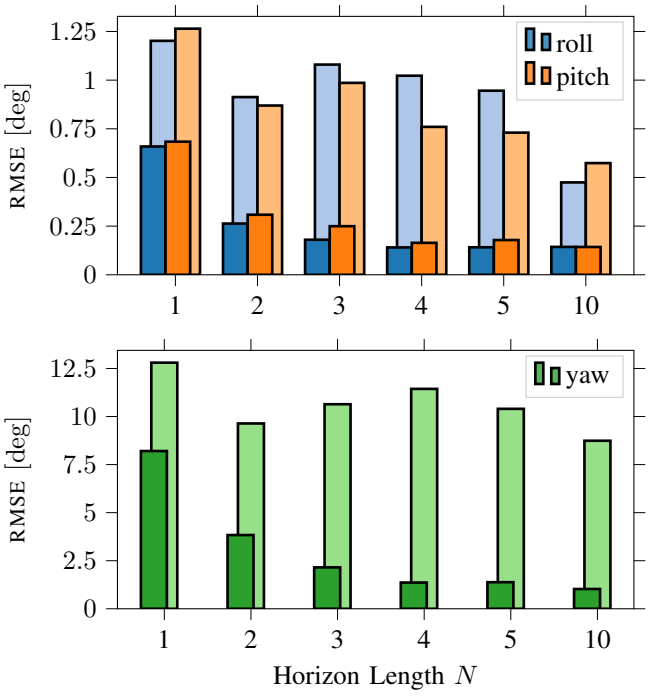

Fig. 3. RMSE of roll and pitch angle (*top*) and yaw angle (*bottom*) of orientation estimates for simulated datasets for different horizon lengths with (*solid-colored*) and without (*light-colored*) the delay estimation enabled. The internally computed quaternion error is plotted in terms of Euler angles for easier interpretation.

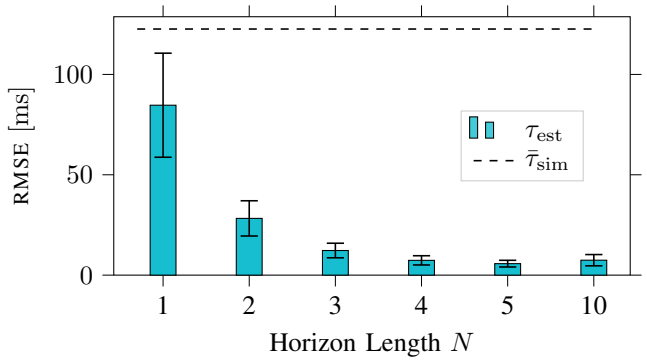

Fig. 4. RMSE of estimated time delay of the GNSS measurements w.r.t to the simulated time delay. The standard deviation of the estimation errors is visualized by the additional error bars. The simulated delay varies for each dataset and its mean value over all datasets is visualized by the dotted line.

the estimated delay for larger horizons, we observe that the RMSE of orientation and position estimates settle already for horizons $N \geq 4$.

V. Experimental Results

The presented approach is evaluated using real measurement data using the experimental setup shown in Fig. 5. The setup consists of three *Xsens MTi 610* IMUs [17] which receive measurement data from a *u-blox ZED-F9* RTK-GNSS receiver [18]. The corresponding datasheet parameters are shown in Table III. An additional GNSS receiver of the same type is used

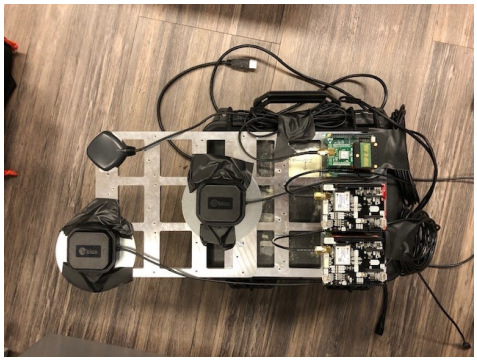

Fig. 5. Experimental setup using three IMUs and three GNSS-RTK receivers with the corresponding antennas. The sensor parameters are shown in Table III.

TABLE III
SENSOR PARAMETERS OF EXPERIMENTAL SETUP.

	Parameter	Value	Unit
Accelerometer	$\mathcal{F}_{\text{acc}}$	400	Hz
	η_{acc}	60	$\mu\text{g}\sqrt{\text{Hz}}^{-1}$
	${}^{\text{S}}_{\text{a}}\delta$	15	μg
Gyroscope	$\mathcal{F}_{\text{gyr}}$	400	Hz
	η_{gyr}	0.007	$\text{deg}\,\text{s}^{-1}\sqrt{\text{Hz}}^{-1}$
	${}^{\text{S}}_{\text{g}}\delta$	8	$\text{deg}\,\text{h}^{-1}$
GNSS	$\mathcal{F}_{\text{gnss}}$	4	Hz
	σ_{gnss}	1	cm
	${}^{\text{S}}\iota$	$[0.3, 0, 0]^{\text{T}}$	m
	τ_{gnss}	180	ms

as base station to provide correction messages to the moving GNSS receivers. The IMU and GNSS share a synchronization signal which allows us to obtain the time of the measurement w.r.t. to the IMU clock despite processing and transmission delays on the GNSS receiver. We used the experimental setup to manually collect several short dynamic trials during which we did random movements while holding the setup. Therefore, we obtain a random trajectory with excitation of all axes.

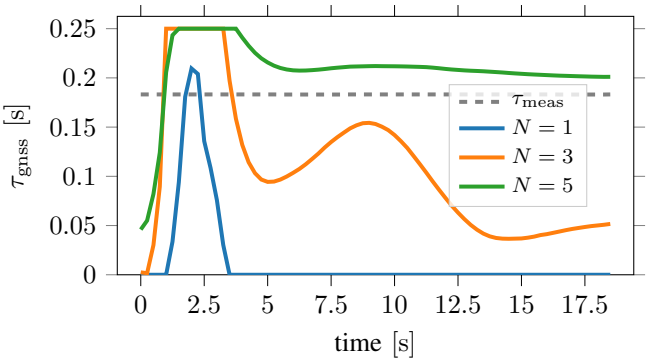

Fig. 6. Comparison of the estimated relative time of measurement and the recorded time of measurement of the GNSS measurements using the experimental setup. The estimates are obtained for different horizon lengths N.

Authorized licensed use limited to: TU Delft Library. Downloaded on March 16,2022 at 12:47:23 UTC from IEEE Xplore. Restrictions apply.

Fig. 6 shows the relative time of measurement for an estimator output rate of 4 Hz. The measured time of measurement τ_{meas} is visualized as a dotted line and was obtained by registering the synchronization pulse of the GNSS receiver. Please note, that τ_{meas} does not represent the processing delay of the receiver itself but instead represents the relative time of measurement in a single collocation interval and expressed in seconds. To relax the assumption of initial knowledge about the time of measurement τ_{gnss}, we initialize τ_{gnss} with the current estimator time. Fig. 6 shows the estimated τ_{gnss} for the horizons $N = \{1, 3, 5\}$. For $N = 1$ a reliable estimation of τ_{gnss} is not possible as τ_{gnss} is estimated with value 0 s. By increasing the horizon, the estimate of τ_{gnss} converges to the measured value τ_{meas}. We obtain the most accurate estimate for $N = 5$. The error at the end of the trial is in the range of 50 ms which is by a magnitude higher compared to the simulation results in Fig.4. The higher error can be explained by parameter errors due to the mechanical uncertainties of the experimental setup. Parameters such as the lever arm ${}^{\mathrm{S}}\iota$ between IMU sensor and GNSS antenna are important quantities for the identification of time delays but are difficult to measure. Earlier work [15] shows, that such uncertain parameters can be estimated online but this exceeds the scope of the paper.

VI. Conclusion & Future Work

In this paper, we presented a novel multi-sensor fusion framework which is able to compensate for unknown time delays of measurements. This is done by finding a continuous-time solution for the estimates allowing us to fuse additional measurement information in an optimal way. The framework is based on a direct collocation approach which specifically addresses sensor fusion problems that rely on nonlinear motion or sensor models. By using a MHE formulation for the resulting estimator, measurements of the past can be integrated up to the length of the estimation horizon. After defining the delay compensation approach in general, it was applied to the problem of GNSS-aided inertial motion tracking estimating.

The estimator was evaluated using simulated motion trajectories and measurement data showing the importance of addressing measurement delays when fusing position measurements with an accuracy of centimeters. Unknown time delays up to 200 ms were compensated with the presented approach reducing the position and orientation errors by one order of magnitude. By using a MHE approach with a measurement horizon $N \geq 4$, we showed a further performance gain in terms of estimation accuracy and stability. Furthermore, we were able to identify the measurement horizon $N = 4$ as a good trade-off between estimation accuracy and computational efficiency for GNSS-aided inertial motion tracking. The practical relevance of the presented approach was shown by estimating and compensating the delay of position measurements in an experimental sensor fusion setup using an IMU and a GNSS-RTK receiver.

In the future, we aim to use the universal multi-sensor fusion framework, described in this paper, for larger multi-sensor fusion setups. By including sensors which process image or pointcloud data, the estimation of processing delays will be particularly interesting. Additionally, we will focus on the improvement of the computational efficiency because the current implementation does not satisfy the real-time constraints. We aim to improve the computational efficiency by exploiting the structure of the MHE estimation problem and finally, we plan to optimize the implementation.

References

[1] L. Mainetti, L. Patrono, and I. Sergi, "A survey on indoor positioning systems," in *Proceedings of the 22nd International Conference on Software, Telecommunications and Computer Networks (SoftCOM)*, 2014, pp. 111–120.

[2] S. Lynen, M. W. Achtelik, S. Weiss, M. Chli, and R. Siegwart, "A robust and modular multi-sensor fusion approach applied to MAV navigation," in *in Proceedings of the IEEE/RSJ International Conference on Intelligent Robots and Systems*, Nov. 2013.

[3] F. Bourgeois, L. Kneip, S. Weiss, and R. Siegwart, "Delay and dropout tolerant state estimation for MAVs," in *Experimental Robotics*. Springer Berlin Heidelberg, 2014, pp. 571–584.

[4] T. D. Larsen, N. A. Andersen, O. Ravn, and N. K. Poulsen, "Incorporation of time delayed measurements in a discrete-time Kalman filter," in *in Proceedings of the 37th IEEE Conference on Decision and Control (CDC)*, vol. 4, 1998, pp. 3972–3977.

[5] A. Gopalakrishnan, N. S. Kaisare, and S. Narasimhan, "Incorporating delayed and infrequent measurements in Extended Kalman filter based nonlinear state estimation," *Journal of Process Control*, vol. 21, no. 1, pp. 119–129, Jan. 2011.

[6] Y. Gu, Y. Chou, J. Liu, and Y. Ji, "Moving horizon estimation for multirate systems with time-varying time-delays," *Journal of the Franklin Institute*, vol. 356, no. 4, pp. 2325–2345, Mar. 2019.

[7] C. V. Rao, J. B. Rawlings, and D. Q. Mayne, "Constrained state estimation for nonlinear discrete-time systems: stability and moving horizon approximations," *IEEE Transactions on Automatic Control*, vol. 48, no. 2, pp. 246–258, 2003.

[8] P. Kühl, M. Diehl, T. Kraus, J. P. Schlöder, and H. G. Bock, "A real-time algorithm for moving horizon state and parameter estimation," *Computers & Chemical Engineering*, vol. 35, no. 1, pp. 71 – 83, 2011.

[9] S. Kameswaran and L. T. Biegler, "Convergence rates for direct transcription of optimal control problems using collocation at radau points," *Computational Optimization and Applications*, vol. 41, no. 1, pp. 81–126, Nov. 2007.

[10] J. L. Crassidis, F. L. Markley, and Y. Cheng, "Survey of nonlinear attitude estimation methods," *Journal of Guidance, Control, and Dynamics*, vol. 30, no. 1, pp. 12–28, 2007.

[11] M. D. Shuster, "Survey of attitude representations," *Journal of the Astronautical Sciences*, vol. 41, no. 4, pp. 439–517, Oct. 1993.

[12] M. Bloesch, H. Sommer, T. Laidlow, M. Burri, G. Nuetzi, P. Fankhauser, D. Bellicoso, C. Gehring, S. Leutenegger, M. Hutter, and R. Siegwart, "A primer on the differential calculus of 3D orientations," 2016.

[13] A. Wächter and L. T. Biegler, "On the implementation of an interior-point filter line-search algorithm for large-scale nonlinear programming," *Mathematical Programming*, vol. 106, no. 1, pp. 25–57, Apr. 2005.

[14] F. Dan Foresee and M. T. Hagan, "Gauss-Newton approximation to Bayesian learning," in *Proceedings of the International Conference on Neural Networks (ICNN'97)*, vol. 3, 1997, pp. 1930–1935.

[15] F. Girrbach, R. Zandbergen, M. Kok, T. Hageman, G. Bellusci, and M. Diehl, "Towards in-field and online calibration of inertial navigation systems using moving horizon estimation," in *Proceedings of the 18th European Control Conference (ECC)*, Jun. 2019, pp. 4338–4343.

[16] S. Łuczak, "Guidelines for tilt measurements realized by MEMS accelerometers," *International Journal of Precision Engineering and Manufacturing*, vol. 15, no. 3, pp. 489–496, Mar. 2014.

[17] *MTi 600-series*, Xsens Technologies B.V. [Online]. Available: https://www.u-blox.com/en/product/zed-f9p-module

[18] *ZED-F9P*, u-blox AG. [Online]. Available: https://www.xsens.com/products/mti-600-series

Authorized licensed use limited to: TU Delft Library. Downloaded on March 16,2022 at 12:47:23 UTC from IEEE Xplore. Restrictions apply.